Optical spectra and energy band structure of single crystalline $CuGaS_2$ and $CuInS_2$

2007 J. Phys.: Condens. Matter 19 456222

(http://iopscience.iop.org/0953-8984/19/45/456222)

J. Phys.: Condens. Matter **19** (2007) 456222 (13pp) doi:10.1088/0953-8984/19/45/456222

Optical spectra and energy band structure of single crystalline $CuGaS_2$ and $CuInS_2$

S Levcenko[1], N N Syrbu[2], V E Tezlevan[1], E Arushanov[1,3], S Doka-Yamigno[3], Th Schedel-Niedrig[3,4] and M Ch Lux-Steiner[3]

[1] Institute of Applied Physics, Academy of Sciences of Moldova, Chisinau, MD 2028, Moldova
[2] Technical University of Moldova, Chisinau, MD-2004, Moldova
[3] Hahn-Meitner Institut GmbH, Glienicker Straße 100, D-14109 Berlin, Germany

E-mail: schedel-niedrig@hmi.de

Received 17 July 2007, in final form 27 September 2007
Published 22 October 2007
Online at stacks.iop.org/JPhysCM/19/456222

Abstract

The reflection spectroscopy of chalcopyrite $CuGaS_2$ and $CuInS_2$ single crystals has been applied for light polarized perpendicular ($E \perp c$) and parallel ($E \parallel c$) to the optical axis in the photon energy range between 1.5 and 6 eV at 77 K. By using the Kramers–Kronig relations, the spectral dependences of the real ε_1 and imaginary ε_2 components of the complex dielectric function $\varepsilon(E) = \varepsilon_1(E) + i\varepsilon_2(E)$ have been calculated for the investigated materials. As a result, the energy band structure of $CuGaS_2$ and $CuInS_2$ at photon energies higher than the fundamental band gap is derived from the analysis of the structures observed in $\varepsilon(\omega)$ spectra. Additionally, the spectral dependences of the complex refractive index, extinction coefficient and absorption coefficient s of $CuGaS_2$ and $CuInS_2$ single crystals are determined in the 1.5–6 eV photon energy range.

1. Introduction

The $CuGaS_2$ (CGS) and $CuInS_2$ (CIS) I–III–VI2 semiconducting compounds crystallize in the chalcopyrite structure belonging to the space group $I\bar{4}2d$-D_{2d}^{12}. Materials of this group have been intensively investigated in the past and are currently used in optoelectronics devices [1, 2]. The energy band structure of these compounds has been calculated as a ternary analog of zinc-blende type semiconductors [3–7]. Transmission, photoluminescence, reflectivity and Raman spectra of $CuGaS_2$ and $CuInS_2$ have also been studied [8–23] previously. An exciton spectrum [15, 24] and emission of biexcitons [21], a resonant Raman scattering of exciton polaritons [17] and an interference of exciton additional waves, as well as a spatial dispersion of exciton polaritons [18, 19], were observed. The energy band structure of $CuGaS_2$ and $CuInS_2$ at

[4] Author to whom any correspondence should be addressed.

photon energies higher than the fundamental band gap has not been well studied [10, 22–24] up to now. The available data sets have been obtained on the basis of ellipsometric investigations on polished samples [22] or, alternatively, by using reflectivity [10, 23, 24] performed on as-grown samples under non-polarized light conditions [24]. It is worth mentioning that the Kramers–Kronig relation for an analysis of the data has not been used up to now and that the observed electronic transitions are currently interpreted only at the points T, Γ and N of the Brillouin zones (BZ) [10, 23, 24] according to theoretical calculations [3, 4].

Recently, the values of the interband energetic distances have been shown at the BZ points T, Γ and N of the calculated band structure of CGS by Laksari *et al* [7]. Additionally, Ahuya *et al* [5] have published a theoretical band structure of CGS along various symmetry directions including not only the T, Γ, N points but also the Z, X and P points of the BZ. This band structure is similar to the published theoretical band structure of Jaffe and Zunger [3, 4], but is calculated along various symmetry directions, which open additional opportunities in the interpretation and localization of the observed electronic transitions.

Reflectivity as well as ellipsometry studies combined with calculations of the optical constants by using the Kramers–Kronig relations are widely used for a determination of the complex dielectric function $\varepsilon(\omega) = \varepsilon_1(\omega) + \mathrm{i}\varepsilon_2(\omega)$ [25, 26]. The structures observed in the $\varepsilon(\omega)$ spectra are attributed to interband critical points (CPs) which are related to regions of the band structure with a huge or a singular point electronic density of states. An accurate knowledge of the dielectric function over a wide range of wavelengths is indispensable for many applications.

In this paper we present reflectivity spectra measured at 77 K and obtained from the mirror-like natural surfaces of as-grown $CuGaS_2$ and $CuInS_2$ single crystals measured in the polarization $E \perp c$ and $E \parallel c$ in the photon energy range of 1.5–6 eV. By using the Kramers–Kronig relations the spectral dependences of the real ε_1 and imaginary ε_2 component of the complex dielectric function ε for $CuGaS_2$ and $CuInS_2$ were calculated. As a result the structure found in the dielectric function was analyzed and related to the electronic band structure of $CuGaS_2$ and $CuInS_2$. The spectral dependences of the complex refractive index, extinction coefficient and absorption coefficient were also determined in the 1.5–6 eV photon energy range.

2. Experimental details

$CuGaS_2$ and $CuInS_2$ crystals in the form of 1 mm thick platelets with surfaces of (0.5×1.5) cm^2 or prisms with $(8 \times 8 \times 4)$ mm^3 sizes were grown from the gas phase in closed quartz ampoules. The reflectivity is measured at 77 K using a Specord M-40 two-beam spectrometer from a (110) surface containing the c [001] axis. The samples were mounted on the cold finger of a vacuum cryostat.

3. Results

3.1. Optical constants

The $CuGaS_2$ and $CuInS_2$ single crystals show well pronounced structures of the reflectivity spectra in the range of $E > E_g$ at 77 K as presented in figure 1. Up to nine peaks are observed in polarization $E \parallel c$ and $E \perp c$. The structure of the reflectivity spectra is richer than that earlier reported [10, 22–24]. By taking into consideration the detected amplitude of the reflection coefficient, it is possible to define a phase of the reflected beam.

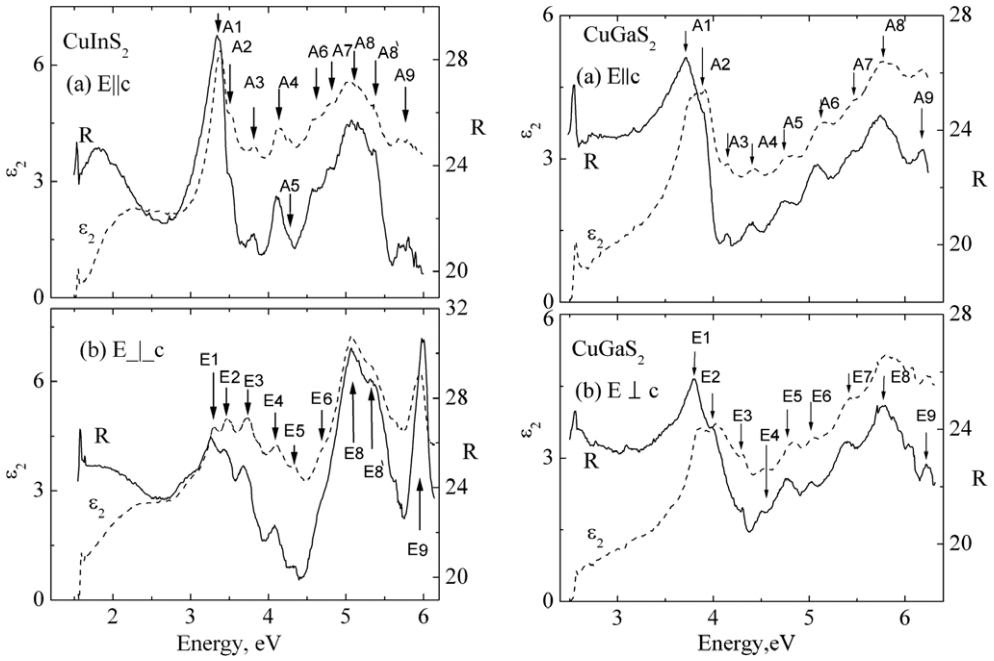

Figure 1. Reflectivity spectra (solid line) and imaginary (ε_2) part (broken line) of the dielectric function versus energy for $CuInS_2$ and $CuGaS_2$ crystals for the polarization $E \parallel c$ (a) and $E \perp c$ (b).

According to [25] and [26], the complex reflectivity r can be described by

$$r = \frac{n - ik - 1}{n - ik + 1} = \sqrt{R}e^{-i\varphi}, \tag{1}$$

where R is the reflectivity, n is the real refractive index, k is the extinction coefficient and φ is the phase angle.

The phase $\varphi(\omega)$ is calculated according to the Kramers–Kronig relations [25, 26] as

$$\varphi(\omega_0) = \frac{\omega_0}{\pi} \int_0^\infty \frac{\ln R(\omega)}{\omega_0^2 - \omega^2} \, d\omega. \tag{2}$$

The value of R is usually determined in the limited range of $a \leqslant \omega \leqslant b$. In our case the measurements have been made between 1.5 and 6 eV. In the high-energy region where measurements of the reflection coefficient are mostly not performed, an approximation of the spectral dependence of the reflection coefficient is used to calculate the dielectric constants by an analytic function which is usually a function of regression of the reflection coefficient.

We have used the approximation for the reflectivity $R(\omega) = R(a)$ for $0 \leqslant \omega \leqslant a$ $(0, a)$ and $R(\omega) = c\omega^{-p}$ for $b \leqslant \omega \leqslant \infty$, where C is constant, and p is constant from [27]. The knowledge of R and $\varphi(\omega)$ permits us to calculate the optical constants as

$$n = \frac{1 - R}{1 - 2\sqrt{R}\cos\varphi + R} \qquad k = \frac{2\sqrt{R}\sin\varphi}{1 - 2\sqrt{R}\cos\varphi + R}$$
$$\varepsilon_1 = n^2 - k^2 \qquad \text{and} \qquad \varepsilon_2 = 2nk. \tag{3}$$

As shown in figures 2–4 for $CuGaS_2$ and $CuInS_2$ single crystals, the spectral dependences of the real ε_1 and imaginary ε_2 components of the complex dielectric function ε and the

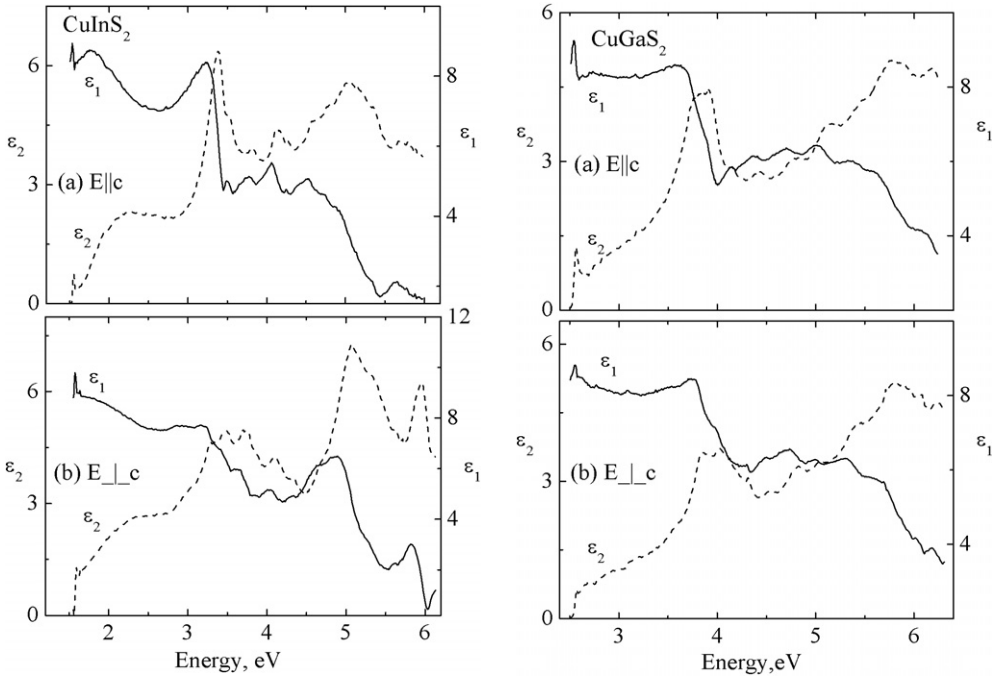

Figure 2. Real (ε_1) and imaginary (ε_2) parts of the dielectric function versus energy for $CuInS_2$ and $CuGaS_2$ crystals.

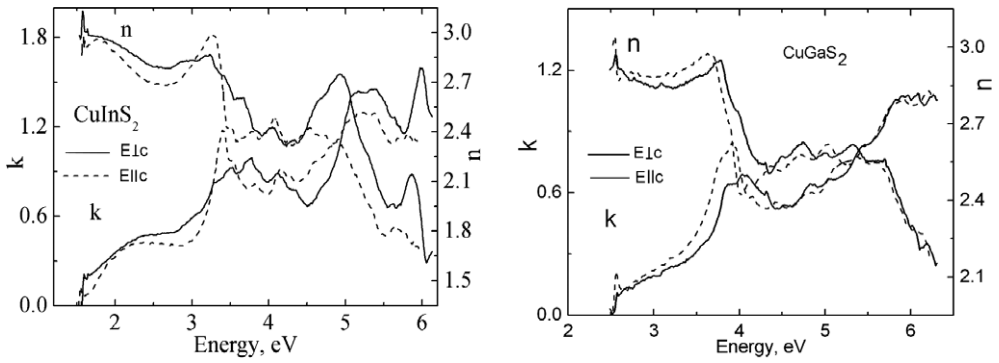

Figure 3. Spectral dependences of the refraction index (n) (real part) and the extinction coefficient (k) for $CuInS_2$ and $CuGaS_2$.

complex refractive index n, as well as the extinction coefficient k, are calculated by using equations (1)–(3). The dependence of the imaginary part ε_2 on energy is given in figure 1 for comparison with the energy dependence of R.

The optical constants of single crystals at 300 K for the materials studied have been determined by Alonso *et al* [22] by means of ellipsometric measurements with polarized light in the range of about 1–5.2 eV. Our data are in a reasonable agreement with the published results, and for $CuGaS_2$ and $CuInS_2$ the well pronounced maxima are observed at about 3.6 eV, 3.3 and 5 eV, respectively, for spectral dependences of ε_1, ε_2, n and k, as well as some small anisotropy mainly of n and k (figure 3). The latter is less pronounced in the high-energy region.

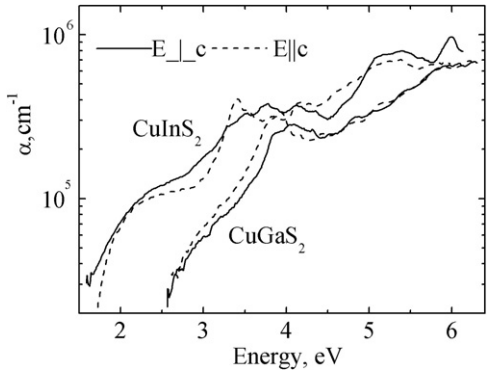

Figure 4. Spectral dependences of the absorption coefficient α for $CuInS_2$ and $CuGaS_2$ crystals.

Furthermore, similar values of n (2.66–2.82 in the range of 1.9–2.5 eV) for $CuGaS_2$ single crystals as well as a small value of its anisotropy (refractive indices of 2.720 and 2.724 for two polarizations at 2.1 eV) are reported by Honeyman and Wilkinson [28]. The values for n and k are published for $CuInS_2$ thin films prepared either (i) by using the thermal evaporation technique—$n = 2.65$–3.05 (0.5–3.0 eV), $k = 0$–1.18 (1.35–3 eV), in [29] and $n = 2.72$–2.95 (0.8–1.4 eV), $k = 0.22$–0.42 (1.7–1.9 eV), in [30]—or (ii) by using the spray method—$n = 2.3$–1.8 and 0.45–0.8 in the range 1.5–4.0 eV in [31]. Some differences between the values published in [28–30] could be due to the usage of different preparation methods. The difference between thin film and single crystal [22] data could be attributed the distinct quality of single crystals and thin films as well as to the roughness of the polished [22] and natural surfaces as shown here.

The real and imaginary parts of the refraction index n and the extinction coefficient k are fundamental optical properties. However, a device physicist who would like to assess the influence of the chalcopyrite optical properties on the solar cell device performance would prefer to know the optical absorption coefficient α. The optical absorption coefficient $\alpha(\lambda) = \frac{4\pi}{\lambda}k(\lambda)$ is presented in figure 4 for $CuGaSe_2$ and $CuInS_2$ crystals, where λ is the wavelength of light in the vacuum. The absorption coefficient shows some anisotropy, mainly below 4.5 eV; at higher energy the anisotropy is negligible.

3.2. Band structure

The structures observed in the $\varepsilon(\omega)$ spectra are attributed to interband critical points (CPs), which are related to regions of the band structure with large or singular point electronic density of states. Here the band structure calculation is needed in order to perform an identification of the observed energy transitions. The band structure of $CuGaS_2$ and $CuInS_2$ has been calculated by Jaffe and Zunger [3, 4] and recently by Ahuya *et al* [5], Lazewski *et al* [6] and Laksari *et al* [7].

Theoretical calculations are performed without taking into account the spin–orbit interaction except in the Ahuya work [5]. The calculations show that at the N point a conduction band N_1 is twofold degenerate. At the N point there are three twofold degenerate valence bands. The transitions at the N point are not polarized in materials with D_{2d} space group if spin–orbit interaction is not taken into account. The spin–orbit interaction changes the selection rules and, hence, the non-polarized transitions become polarized.

These degenerate bands should be split and accordingly each pair splits into two bands if the spin–orbit interactions are taken into account. Hence, at the N point of the BZ, one observes two upper pairs of the V band assigned to $4V$ bands, and also the lower conduction band N_1 is split into two bands. In this case the eight polarized electronic transitions can be found at point N. According to the theoretical calculation [3, 4, 6, 7] at point Γ of the BZ, the upper valence band is twofold degenerate, while the lower valence band is threefold degenerate. The conduction band is doubly degenerate at the Γ point. The spin–orbit interaction can lead to a splitting of the valence band and the conduction band at the Γ point, which could be responsible for the anisotropy of the optical spectra.

The valence bands at points Z, X and P of the BZ are also degenerate. For the crystalline systems these bands are found to split and to cause the polarized electronic transitions which could be observed in the structures of the reflectivity spectra. For example, the two upper valence bands V_1 and V_2 are presented at the Z point of the band structure diagram. Each of these bands is twofold degenerate and, as a result, four electronic transitions appear in the vicinity of point Z within a narrow energy interval, which are assigned to the C_1 conduction band (figure 8). A similar situation is also found at other points of the BZ. Subsequently, one can assume that a lifting of the degeneration of V_1 bands at any point of the BZ will lead to the occurrence of some additional peaks A_i and E_i with polarization $E \parallel c$ and $E \perp c$ in the reflectivity spectra.

The knowledge of the band structure permits us to determine ε_2, the theoretical spectral dependence. A criterion of correctness of the calculated band structures is the conformity of theoretical spectral dependence with the ε_2 experimental spectral dependence. The ε_2 structure of the latter can be analyzed in terms of the standard analytic line shapes [25]

$$\varepsilon(\omega) = C - A\mathrm{e}^{\mathrm{i}\varphi}(\omega - E + \mathrm{i}\gamma)^m, \tag{4}$$

where A is the critical-point parameter amplitude, E is the energy threshold, γ is the broadening and φ is the phase angle. In order to enhance the structural features presented in the $\varepsilon(\omega)$ spectra and to obtain the CP parameters, the second-derivative spectrum of the complex dielectric function, $\frac{\mathrm{d}^2\varepsilon(\omega)}{\mathrm{d}\omega^2}$, is numerically calculated from our ε data with a standard technique of polynomial smoothing. The parameters A, E, γ and φ are determined by fitting the numerically obtained second-derivative spectra of the experimental $\varepsilon(\omega)$ to equation (4). The exponent m is equal to $-1/2$ and $1/2$ for one- (1D) and three-dimensional (3D) CPs, respectively. In the case of two-dimensional (2D) CPs one obtains with $m = 0 : \varepsilon(\omega) = C - A\mathrm{e}^{\mathrm{i}\varphi}\ln(\omega - E + \mathrm{i}\gamma)$. Discrete excitons with Lorentzian line shape (0D) are represented by $m = -1$. Due to the fact that CPs are directly related to regions of large or singular joint electronic density of states, direct information can be obtained on the energy separation of valence and conduction bands (interband gaps), which can be compared with the band-structure calculations [25].

The second derivative of the complex dielectric function (SD) can be written as [32]

(a) for $m \neq 0$,

$$\frac{\mathrm{d}^2\varepsilon}{\mathrm{d}\omega^2} = A'(\Omega)^{(m-2)/2}\left\{\cos\left[(m-2)\arccos\left(\frac{\omega - E}{\Omega^{1/2}}\right) + \varphi\right] + \mathrm{i}\sin\left[(m-2)\arccos\left(\frac{\omega - E}{\Omega^{1/2}}\right) + \varphi\right]\right\} \qquad \text{with } A' = -m(m-1)A,$$
$$\Omega = (\omega - E)^2 + \gamma^2; \tag{5a}$$

(b) for $m = 0$,

$$\frac{\mathrm{d}^2\varepsilon}{\mathrm{d}\omega^2} = \frac{A}{\Omega}\left\{\cos\left[-2\arccos\left(\frac{\omega - E}{\Omega^{1/2}}\right) + \varphi\right] + \mathrm{i}\sin\left[-2\arccos\left(\frac{\omega - E}{\Omega^{1/2}}\right) + \varphi\right]\right\}. \tag{5b}$$

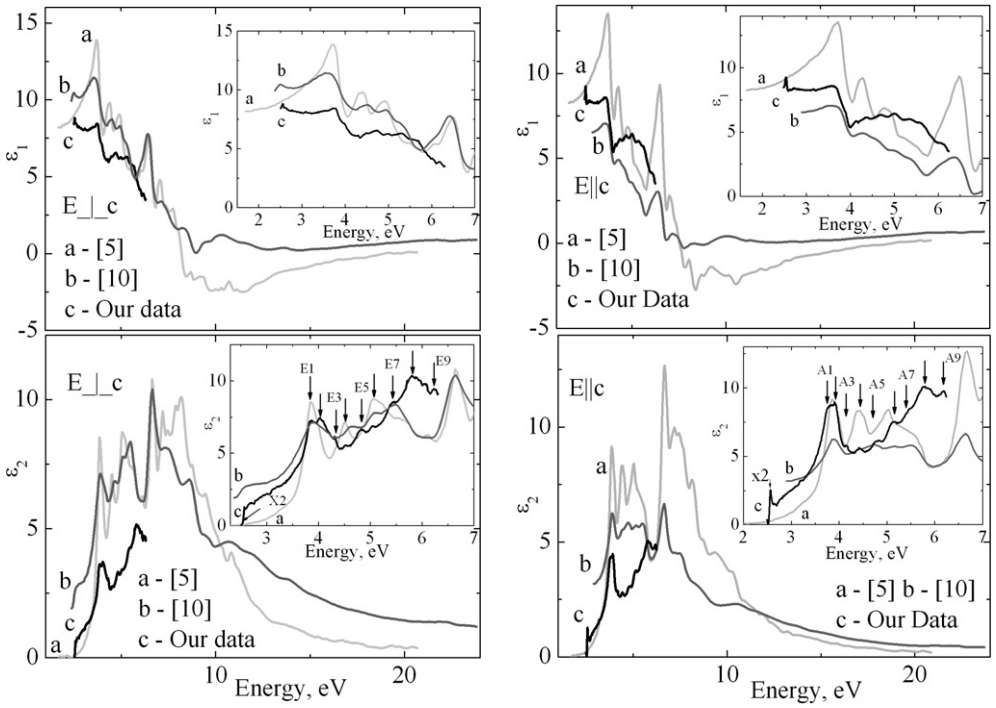

Figure 5. Real (ε_1) and imaginary (ε_2) parts of the dielectric function versus energy for $CuGaS_2$ crystals. Experimental [10] and theoretical [5] spectral dependences of the real ε_1 and imaginary ε_2 parts for $CuGaS_2$ calculated using experimental [10] and theoretical [5] reflectivity spectra are also presented. Data of [5] are displaced by 1.2 eV, which corresponds to the difference between theoretical [5] and experimental values [1] of the fundamental gap.

This method (we will name it SDM) was successfully applied to different semiconducting materials in order to identify and evaluate the energy of the electronic transitions [25, 32–35].

4. Discussion

The spectral dependences of ε_1, ε_2, n, k and α are found for $CuGaS_2$ and $CuInS_2$ single crystals (figures 1–4) to reveal distinct structures at the critical points.

Our reflectivity spectral measurements are performed in a relatively narrow energy range between 1.5 and 6 eV. Spectral dependences of the real ε_1 and imaginary ε_2 parts of the dielectric function are calculated in the same range with an approximation in the ultraviolet region. In order to check the correctness of our calculations, the data are compared with the experimental [10] and theoretical [5] spectral dependences of ε_1 and ε_2 as shown in figure 5 for $CuGaS_2$. This is done by calculating experimental [10] and theoretical [5] reflectivity spectra which are obtained in a wider range of energy (from 1 to 20–25 eV). Our measurements have been performed in the 1.5–6 eV photon energy range. We found a reasonable agreement of the $\varepsilon_1(\varepsilon_2)$ calculated spectra with our results in the range 1.5–6 (1.5–5.5) eV. The data given in [10] are displaced by 1.2 eV, as pointed out by Ahuya *et al* [5], which corresponds to the difference between the theoretical [5] and experimental values of the fundamental gap.

The experimental spectra of the imaginary $\varepsilon_2(\omega)$ and real $\varepsilon_1(\omega)$ components of the complex dielectric function $\varepsilon(\omega)$ show peaks for the $CuGaS_2$ and $CuInS_2$ single crystals

Table 1. Transition energies (eV) determined from the reflectivity spectra, the fit parameters $/E$, the energy threshold (eV) and γ, the broadening (eV), of the CPs and localization of transitions for CIS and CGS samples.

			$CuGaS_2$				
A_1	R	3.71	$\Gamma_7(V_1)$–$\Gamma_7(C_2)$	A_6	R	5.08	$X(V_2)$–$X(C_1)$
	ε	3.72(1)			ε	5.04(1)	
	γ	0.07(1)			γ	0.10(1)	
E_1	R	3.80		E_6	R	5.02	
	ε	3.82(1)			ε	5.00(2)	
	γ	0.06(1)			γ	0.05(2)	
A_2	R	3.91	$\Gamma_6(V_2)$–$\Gamma_7(C_2)$	A_7	R	5.41	$N(V_1)$–$N(C1)$
	ε	3.97(1)	or		ε	5.32(2)	
	γ	0.07(1)	$\Gamma_7(V_3)$–$\Gamma_7(C_2)$		γ	0.10(2)	
E_2	R	3.98		E_7	R	5.40	
	ε	3.99(1)			ε	5.35(1)	
	γ	0.04(1)			γ	0.09(1)	
A_3	R	4.14	$Z(V_1)$–$Z(C_1)$	A_8	R	5.74	$N(V_2)$–$N(C_1)$
	ε	4.12(2)	or		ε	5.74(3)	
	γ	0.04(2)	$P(V_1)$–$P(C_1)$		γ	0.14(3)	
E_3	R	4.30		E_8	R	5.71	
	ε	4.36(1)			ε	5.72(2)	
	γ	0.04(1)			γ	0.1(1)	
A_4	R	4.38	$Z(V_2)$–$Z(C_1)$	A_9	R	6.18	$N(V_3)$–$N(C_1)$
	ε	4.39(1)	or		ε	6.17(2)	
	γ	0.07(1)	$P(V_2)$–$P(C_1)$		γ	0.07(1)	
E_4	R	4.51		E_9	R	6.23	
	ε	4.52(2)			ε	6.19(2)	
	γ	0.05(2)			γ	0.06(2)	
A_5	R	4.74	$X(V_1)$–$X(C_2)$				
	ε	4.71(3)					
	γ	0.07(2)					
E_5	R	4.77					
	ε	4.78(1)					
	γ	0.08(1)					

(figure 2) corresponding to the critical points (CPs) of energy transitions in the electronic band structure. The accurate values of the energy thresholds have been determined by the theoretical fitting of the second derivative. The obtained fitting parameters (threshold energy and broadening) are compiled in table 1.

Figures 6 and 7 show the second derivative with respect to the photon energy of the experimental real and imaginary components of the dielectric function, $d^2\varepsilon_2/d\omega^2$ and $d^2\varepsilon_1/d\omega^2$. Theoretical fittings are also shown according to SDM. These fitting have been obtained by considering CPs as 2D with $m = 0$.

A band structure calculation is available for $CuGaS_2$ and $CuGaS_2$ [3–7] and is used to identify the energy transitions observed. The assignment of experimental peaks of ε_1 and ε_2 is performed by taking into account the results of theoretical calculations.

For $CuGaS_2$ crystals, one observes intensive peaks in the range of $E > E_g$ for the dielectric function and the reflectivity spectra labeled A_1 (3.72 and 3.71 eV) and E_1 (3.82 and 3.80 eV) in the polarization $E \parallel c$ and $E \perp c$, respectively (figure 1). For $CuInS_2$ crystals the shape of the

Table 1. (Continued.)

$CuInS_2$							
A_1	R	3.34	$\Gamma_7(V_1)$–$\Gamma_7(C_2)$	A_6	R	4.60	$X(V_2)$–$X(C_1)$
	ε	3.40(1)			ε	4.55(1)	
	γ	0.07(1)			γ	0.06(1)	
E_1	R	3.26		E_6	R	4.70	
	ε	3.266(7)			ε	4.61(1)	
	γ	0.06(1)			γ	0.09(2)	
A_2	R	3.51	$\Gamma_6(V_2)$–$\Gamma_7(C_2)$	A_7	R	4.79	$N(V_1)$–$N(C_1)$
	ε	3.57(3)	or		ε	4.80(2)	
	γ	0.04(3)	$\Gamma_7(V_3)$–$\Gamma_7(C_2)$		γ	0.04(2)	
E_2	R	3.46					
	ε	3.49(3)					
	γ	0.06(2)					
A_3	R	3.81	$Z(V_1)$–$Z(C_1)$	A_8	R	5.07	$N(V_2)$–$N(C_1)$
	ε	3.83(1)	or		ε	4.97(1)	
	γ	0.06(1)	$P(V_1)$–$P(C_1)$		γ	0.10(1)	
E_3	R	3.68		E_8	R	5.06	
	ε	3.70(2)			ε	5.04(1)	
	γ	0.08(2)			γ	0.12(1)	
A_4	R	4.11	$Z(V_2)$–$Z(C_1)$	A_9	R	5.68	$N(V_3)$–$N(C_1)$
	ε	4.10(1)	or		ε	5.62(2)	
	γ	0.07(1)	$P(V_2)$–$P(C_1)$		γ	0.1	
E_4	R	4.08		E_9	R	5.98	
	ε	4.06(1)			ε	5.93(2)	
	γ	0.08(1)			γ	0.11(2)	
A_5	R	4.26	$X(V_1)$–$X(C_1)$				
	ε	4.32(1)					
	γ	0.06(1)					
E_5	R	4.32					
	ε	4.29(2)					
	γ	0.05(2)					

dielectric function and the reflectivity features is almost identical to that of crystalline $CuGaS_2$ and, therefore, the features are assigned to identical indices. Hence, the $CuGaS_2$ system is studied in more detail and the identification of the spectra will be done on the basis of data of this material, but the conclusions will be made for both crystals. The peaks A_1 (3.72 and 3.71 eV) and E_1 (3.82 and 3.80 eV) are analogues of peaks ($E_1(A)$) with values 3.72 ($E \parallel c$) and 3.85 eV ($E \perp c$) observed in the ellipsometric spectra at 300 K [22]. According to [10], reflectivity peaks occurred at 3.84 ($E \parallel c$) and 3.82 eV ($E \perp c$). These peaks are assigned as $N_1(V_1)$-to-$N_1(C_1)$ transitions [22, 24] and the interpretation is based on theoretical band structure calculations performed at three actual points of the BZ, namely Γ, T and N [3, 4].

Our experimental results are analyzed on the basis of theoretical band structure calculations from [5] at the actual points X, P, Z, N and Γ of the BZ. The reasonable agreement of the theoretical spectral function, $\varepsilon_2(\omega)$ [5], with our experimentally observed spectral dependences of $\varepsilon_2(\omega)$ in almost all the range of our experimental study (from 1.5 to 5–5.5 eV; measurements were performed up to 6 eV) (figure 5) is a hint at the reliability of the calculated band structures [5]. For an interpretation of the reflectivity spectra, we will consider the band diagrams [5] only in the range of minima of an interband interval (figure 8) under the

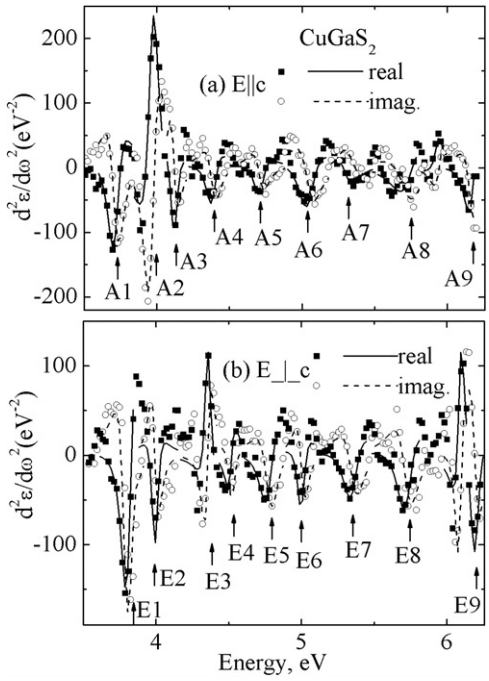

Figure 6. Second numeral derivative spectra of the real (ε_1) and imaginary (ε_2) parts of the dielectric function for $CuGaS_2$ crystals and the theoretical fitting using the SDM method.

preservation of the scale for all points of the BZ. The lowest energy interval $\Gamma_7(V_1)$ to $\Gamma_6(C_1)$ is conditionally designated to E_0 (2.5 eV), which corresponds to the value of the fundamental gap of $CuGaS_2$ at low temperatures [1]. For further discussion we estimate the vertical interband energetic distance at other points of the BZ in units of E_0. As a result of these estimations it is found that the energetic distance $\Gamma_7(V_1)$ to $\Gamma_7(C_2)$ is equal to $1.87E_0$, which gives the lowest value compared to the points Z, X, P and N at the BZ. Hence, it is reasonable to assume that peaks A_1 and E_1 shown in figure 6 are caused by transitions at the Γ point from V_1 to C_2. For the $CuInS_2$ crystals these features are also localized at the Γ point, due to transitions from the upper valence band to the conductivity band [23] as shown in figure 7. The features A_2 (3.97 and 3.91 eV) and E_2 (3.99 and 3.98 eV) can be observed for polarizations of $E \parallel c$ and $E \perp c$, respectively, at somewhat higher transition energies, as given in figure 6. The energetic positions of peaks A_2 and E_2 are separated from A_1 and E_1 approximately by the valence band splitting in the center of the BZ due to a crystal field and spin–orbit interaction. The V_2–V_3 splitting due to a spin–orbit interaction is small and not observed in our spectra. It permits us to assign peaks A_2 and E_2 as transitions in the center of the BZ from the valence band $\Gamma_6(V_2)(\Gamma_7(V_3))$ to the conductivity band $\Gamma_7(C_2)$.

Peaks A_3 (4.12 and 4.14 eV), E_3 (4.36 and 4.30 eV) and A_4 (4.39 and 4.38 eV), E_4 (4.52 and 4.51 eV) are observed for the polarization $E \parallel c$ and $E \perp c$, respectively, in figure 6. Peaks A_3 (4.15 eV) and A_4 (4.38 eV) are attributed to the transitions of $N_1(V_3)$ to $N_1(C_1)$ and $\Gamma_7(V_1)$ to $\Gamma_7(C_2)$ and are observed for non-polarized light [24]. These peaks correspond to those $(E_1(\Delta X))$ observed in the ellipsometric spectra at 300 K as given in [22] with values of 4.15 eV at $E \parallel c$ and are related to the $(T3v + T4v) - (T1c + T2c)$ pseudo-direct transition. According to [5], the vertical energetic distance between the upper valence band and the lower conduction band in the vicinity of the P, Z and N points is equal to 2.04 and

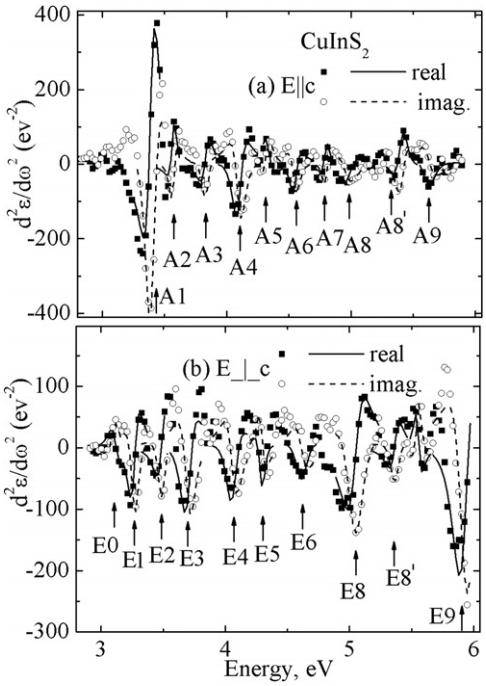

Figure 7. Second numeral derivative spectra of the real (ε_1) and imaginary (ε_2) parts of the dielectric function for CIS and the theoretical fitting using SDM.

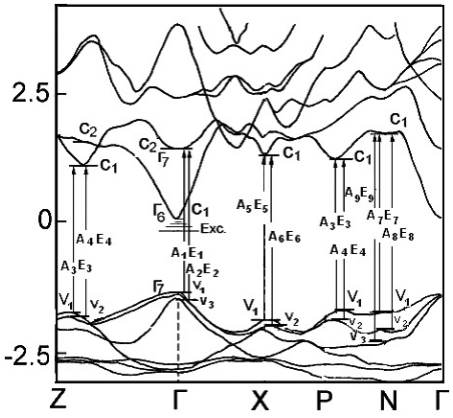

Figure 8. Proposed assignment and notations for the transitions in $CuInS_2$ and $CuGaS_2$ crystals, depicted on a generic band structure.

$2.43E_0$, respectively. The former distance of $2.04E_0$ is sufficiently lower than that at the N and X points of the BZ. By taking this into account we can assume that the peaks A_3 (4.12 and 4.14 eV), E_3 (4.36 and 4.30 eV), and A_4 (4.39 and 4.38 eV), E_4 (4.52 and 4.51 eV), are caused by transitions at the P or Z point.

At 5 eV, peaks A_5 (4.71/4.74 eV) and E_5 (4.78/4.77 eV) are observed for the polarization of $E \parallel c$ and $E \perp c$, respectively. Peak A_5 (4.73 eV) is attributed to transitions at $\Gamma_6(V_2)$ to

$\Gamma_7(C_2)$ and is observed for non-polarized light [24]. In [10] the reflectivity spectral features are found at 4.70 eV ($E \parallel c$) and 4.68 eV ($E \perp c$). These peaks correspond to those bands ($E_1(B)$) as observed in the ellipsometric spectra at 300 K [22] with values of 4.63 eV ($E \parallel c$) and 4.53 eV ($E \perp c$), respectively, and are assigned to $N_1(V_2)$–$N_1(C_1)$ transitions. By taking into account that the energetic separation at the X point is larger than at the P and $pointsZ$ but smaller than at the N point we can attribute the localized peaks A_5 (4.71 and 4.74 eV) and E_5 (4.78 and 4.77 eV) at the X point to transitions from V_1 to C_1.

Peaks A_6 (5.04 and 5.08 eV) and E_6 (5.00 and 5.02 eV) observed at the polarization $E \parallel c$ and $E \perp c$, respectively, could be caused by V_2–(C_1) transitions at the X point as reported in [24], where A_6 is observed at 5.16 eV. These peaks probably agree with those observed in the reflectivity spectra as presented in [10] at 5.14 ($E \parallel c$) and 5.12 eV ($E \perp c$), respectively. It is worth mentioning that a feature at 4.91 eV ($E \perp c$) ($E_1(B)$) in the ellipsometric spectra at 300 K given in [22] is assigned to a $\Gamma_4(V_2)$-to-$\Gamma_1(C_1)$ transitions at the Γ point. Such a difference is caused by some differences between the band structure used for the transition identifications in our paper and in [22]. Our experimental results are analyzed on the basis of theoretical band structure calculations from [5] at the actual X, P, Z, N and Γ points of the BZ. In [22] the observed electronic transitions are interpreted only at the T, Γ and N points of the Brillouin zone (BZ) according to theoretical calculations [3, 4].

Peaks A_7 (5.32 and 5.41 eV) and E_7 (5.35 and 5.40 eV) are observed for the polarization $E \parallel c$ and $E \perp c$, respectively. The interband energetic distance at the N point is equal to $2.43E_0$, and is found to be smaller than the distance at the Γ point according to the theoretical calculation of [3] and [4] but larger than the interband distance at the X, P and Z points [5]. We assume that peaks A_7 and E_7 are caused by transitions from V_1 to C_1 at the N point or, alternatively, by a V_1–C_1 transition at the Γ point according to [24].

Peaks A_8 (5.74 and 5.74 eV) and E_8 (5.72 and 5.71 eV) are observed for polarization $E \parallel c$ and $E \perp c$, respectively, and are caused probably by transition V_2–C_1 at the N point or V_2–C_1 at the Γ point as reported for A_7 (5.65 eV) in [24]. At an energy of 6 eV, peaks A_9 (6.17 and 6.18 eV) and E_9 (6.19 and 6.23 eV) are observed for the polarization $E \parallel c$ and $E \perp c$, respectively. These peaks can also be attributed to V_3–C_1 transitions at the N point. It is worth mentioning that the observation of peaks $A_{8'}$ (5.41 and 5.37 eV) and $E_{8'}$ (5.37 and 5.32 eV) in $CuInS_2$ is probably caused by transitions at the N point, too.

In table 1 the values of the electronic transitions above the fundamental gap for the compounds are summarized. Figure 8 presents a schematic representation of the energy levels and transitions that contribute to the measured dielectric function for CGS and CIS.

5. Conclusions

Reflection spectroscopy has been used to determine the pseudo-dielectric functional spectra of single crystalline $CuGaS_2$ and $CuGaS_2$ grown by chemical vapor transport. The measured $\varepsilon(\omega)$ spectra reveal a large number of structures attributed to transitions at the interband critical points. The structures observed have been analyzed by using the second derivative of the complex dielectric function. The model used here permits us to obtain a successful agreement with our experimental results of the $\varepsilon(\omega)$ dielectric function within the accuracy of the measurement. The values of the interband critical-point parameters (threshold energy and broadening) have been derived from the applied models. The analysis of the dielectric function allows us to identify and to evaluate the energy positions of almost nine electronic transitions. In addition, the spectral dependences of the complex refractive index, the extinction coefficient and the absorption coefficient of $CuGaS_2$ and $CuGaS_2$ single crystals are determined in the 1.5–6 eV photon energy range.

Acknowledgment

Financial support from INTAS program (project 03-51-6314) is acknowledged.

References

[1] Shay J L and Wernick J H 1975 *Ternary Chalcopyrite Semiconductors: Growth, Electronic Properties, and Applications* (Oxford: Pergamon)
[2] Birkmire R W and Eser E 1997 *Annu. Rev. Mater. Sci.* **27** 625
[3] Jaffe J E and Zunger A 1983 *Phys. Rev.* B **28** 5822
[4] Jaffe J E and Zunger A 1984 *Phys. Rev.* B **29** 1882
[5] Ahuya R, Auluck S, Eriksson O, Wills J M and Johansson B 1998 *Sol. Energy Mater. Sol. Cells* **53** 357
[6] Lazewski J, Jochym P T and Parlinski K 2002 *J. Chem. Phys.* **117** 2726
[7] Laksari S, Chahed A, Abbouni N, Benhelal O and Abbar B 2006 *Comput. Mater. Sci.* **38** 223
[8] Metzner H, Eberhardt J, Cieslak J, Hahn Th, Goldhahn R, Reislöhner U and Witthuhn W 2004 *Thin Solid Films* **451/452** 241
[9] Syrbu N N, Khachaturova S B, Bodnar I V and Rabotinskii N D 1989 *Opt. Spectrosc.* **66** 693
[10] Rife J C, Dexter R N, Bridenbaugh P M and Veal B W 1977 *Phys. Rev.* B **16** 4491
[11] Tsuboi N, Kobayashi S, Kaneko F and Maruyama T 1988 *Japan J. Appl. Phys.* **27** 972
[12] Shirakata S and Chichubu S 2000 *J. Appl. Phys.* **87** 3793
[13] Susaki M, Yamamoto N, Pervot B and Schwab C 1996 *Japan. J. Appl. Phys.* **35** 1652
[14] Yamamoto N, Kitakuni M and Susaki M 1995 *Japan. J. Appl. Phys.* **34** 3019
[15] Yakushev M V, Mudryi A V, Feofanov Y, Ivaniukovich A V and Viktorov I V 2006 *Thin Solid Films* **511/512** 130
[16] Terasako T, Umiji H, Tanaka K, Shirakata S, Uchiki H and Isomura S 1999 *Japan. J. Appl. Phys.* **38** L805
[17] Syrbu N N, Blaje M A, Tiginyanu I M and Tezlevan V E 2002 *Opt. Spectrosc.* **92** 395 (in Russian)
[18] Syrbu N N, Ursaki V V, Tiginyanu I M, Tezlevan V E and Blaje M A 2003 *J. Phys. Chem. Solids* **64** 1967
[19] Syrbu N N, Blaje M A, Tezlevan V E and and Ursaki V V 2002 *Opt. Spectrosc.* **92** 402
[20] Radautan S I, Syrbu N N, Cretu R V and Tezlevan V E 1997 *Proc. 20th Int. Semicond. Conf. (Sinaia, Oct., 1997)*
[21] Tanaka K, Uchiki H, Iida S, Terasako T and Shirakata S 2000 *Solid State Commun.* **114** 197
[22] Alonso M I, Wakita K, Pascual J, Garriga M and Yamamoto N 2001 *Phys. Rev.* B **63** 075203
[23] Syrbu N N, Cretu R V and Tezlevan V E 1998 *Cryst. Res. Technol.* **33** 135
[24] Syrbu N N, Tiginyanu I M, Nemerenko L L, Ursaki V V, Tezlevan V T and Zalamai V V 2005 *J. Phys. Chem. Solids* **66** 1974
[25] Lautenschlager P, Garriga M, Logothetidis S and Cardona M 1987 *Phys. Rev.* B **35** 9174
Cardona M 1969 *Modulation Spectroscopy* (New York: Academic)
[26] Kalugin A I and Sobolev V V 2005 *Phys. Rev.* B **71** 115112
Sobolev V and Nemoshkalenko V 1988 *Methods of Computational Physics in Solid State Theory. Electronic Structure of Semiconductors* (Kiev: Naukova Dumka)
[27] Philipp H R and Taft E A 1959 *Phys. Rev.* **113** 1002
[28] Honeyman W N and Wilkinson K H 1971 *J. Phys. D: Appl. Phys.* **4** 1182
[29] El-Nahass M M, Soliman H S, Kadry N El, Morsy A Y and Yaghmour S 1988 *J. Mater. Sci. Lett.* **7** 1050
[30] Zribi M, Kanzari M and Rezig B 2006 *Mater. Lett.* **60** 98
[31] Kamoun M, Bennaceur R and Frigerio J M 1994 *J. Physique* III **4** 983
[32] Albornoz J G, Serna R and Leon M 2005 *J. Appl. Phys.* **97** 103515
[33] Alonso M I, Garrida M, Durante Rincon C A and Leon M 2000 *J. Appl. Phys.* **88** 5796
[34] Alonso M I, Wakita K, Pascual J, Garriga M and Yamamoto N 2001 *Phys. Rev.* B **63** 075203
[35] León M, Levcenko S, Nateprov A, Nicorici A, Merino M, Serna R and Arushanov E 2007 *J. Phys. D: Appl. Phys.* **40** 740